THE PENNSYLVANIA STATE UNIVERSITY
SCHREYER HONORS COLLEGE

DEPARTMENT OF AEROSPACE ENGINEERING

VIBRATION DAMPING OF ALUMINUM PLATES USING ACOUSTIC BLACK HOLES FOR APPLICATION IN AEROSPACE STRUCTURES

ANGELINA M. CONTI
SPRING 2016

A thesis
submitted in partial fulfillment
of the requirements
for a baccalaureate degree
in Aerospace Engineering
with honors in Aerospace Engineering

Reviewed and approved* by the following:

Stephen C. Conlon
Associate Professor of Aerospace Engineering
Senior Research Associate, PSU Applied Research Laboratory
Thesis Supervisor

Dennis K. McLaughlin
Professor of Aerospace Engineering
Honors Adviser

* Signatures are on file in the Schreyer Honors College.

ABSTRACT

In recent years, scientists have investigated the acoustic black hole (ABH) effect as a low-weight high-performance vibration control device for application in aerospace structures. The ABH effect uses a specific power-law skin thickness taper to decrease the velocity of an incident bending wave to nearly zero. Once the velocity has decreased, the wave is unable to reflect back at the far edge, thus trapping it in the ABH. Applying a small amount of viscoelastic damping material to the surface of the ABH dissipates most of the vibration while adding very little weight and cost to the overall structure. Experimental tests prove that the ABH is an effective way to trap and damp vibration energy. The ABH effect is quantified through experimental broadband vibration response comparisons between three aluminum plates of varying degree of vibration control and damping. In general, the low-frequency responses were very similar among all three plates since global modes dominate the response. After the cut-on frequency of the ABH was reached, the ABH effect induced a large variation in the surface averaged mobility, explained by the focusing of energy in the ABH cells. The application of damping material decreased the surface averaged mobility and its variation. Increasing the frequency also decreased the surface averaged mobility variation. These experiments proved that the ABH effect successfully focuses vibration energy from the plate to the center of the two-dimensional ABH and that the added layer of damping material effectively reduces the vibration energy of the structure, while adding very little weight. The ABH could potentially replace traditional heavy and inefficient acoustic treatments, increasing the fuel efficiency by decreasing the weight devoted to acoustic treatment. Future work will include testing an “add-on” ABH device for application in existing airframes.

TABLE OF CONTENTS

LIST OF FIGURES

LIST OF TABLES

ACKNOWLEDGEMENTS

I would like to thank my thesis advisor Dr. Stephen C. Conlon for the time and effort he spent guiding me through this research project. Over the past four years, he led me through several experimental investigations of topics related to structural vibrations in preparation for this thesis. The entire experience has been extremely rewarding, and I hope to continue experimental work in the future. I would also like to thank my honors advisor Dr. Dennis K. McLaughlin for his guidance and support through my academic and career decisions over the past four years. Finally, I would like to thank Philip Feurtado for his guidance with the laboratory experiments.

Chapter 1

Introduction

1.1 Background

One of the main areas of optimization in the field of aircraft design is the overall weight efficiency of the structure. NBC[24] points out that each pound shed from a commercial transport airplane saves 14,000 gallons of fuel per year. Creating a weight efficient airplane involves balancing the weight, structural strength, safety and utility of systems on an airplane. One area in need of improvement is the weight efficiency of the acoustic treatment. The intense structural vibrations from the propulsion system of aircraft must be controlled to prevent structural damage and decrease cabin and community noise impacts. Traditional vibrational damping methods place acoustic treatment patches at various locations on the airframe to reduce the local vibration energy. Typically, a large amount of acoustic treatment is required to dissipate the vibration energy enough to create a safe airplane that meets FAA noise regulations. This often adds a significant amount of weight to the structure, ultimately reducing its fuel efficiency.

In the past decade, scientists have explored a new concept that can focus the vibration energy of a structure to discrete locations on the airframe. Applying a small amount of damping material to these locations will dissipate most of the vibration energy of the structure, while only adding a small amount of weight compared to traditional methods. This concept, called the acoustic black hole (ABH) effect, has the potential to save a significant amount of weight on an aircraft, ultimately increasing its fuel efficiency.

Investigations of the ABH effect reveal that a very specific power-law skin thickness taper can decrease the incident bending wave speed in a thin plate to nearly zero, given by

$$c_b = \left(\frac{Eh(x)^2\omega^2}{12\rho(1-\nu^2)}\right)^{1/4}, \quad (1)$$

where c_b is the bending wave speed, ρ is the density, ω is the angular frequency, E is the Young's Modulus, υ is the Poisson's ratio, and h(x) is the thickness profile. As the plate thickness tapers to zero, the velocity of the bending wave theoretically approaches zero. Once the velocity has decreased, the wave is unable to reflect back at the far edge and is therefore "trapped" in the acoustic black hole, conceptually drawn in Figure 1.

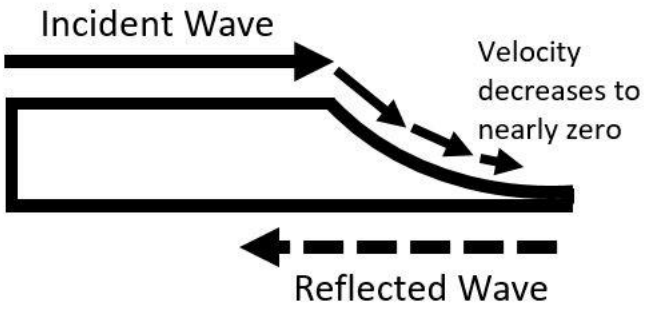

Figure 1. Diagram of the acoustic black hole effect, where the incident bending wave velocity decreases proportionally to skin thickness and is therefore unable to reflect.

This creates a unique opportunity for acousticians since much of the structure's vibration energy is now focused at discrete locations. Applying a small amount of viscoelastic damping material to the surface of the thickness taper (ABH) will dissipate the vibration while adding very little weight and cost to the overall structure. This is great news in the weight- and cost-dependent field of aviation. Instead of traditionally applying acoustic treatment patches to the entire structure with limited damping efficiency, designers can apply a small amount to a grid of ABH cells, increasing the vibration reduction while saving significant weight and cost. The Center of

Acoustics and Vibration at the Pennsylvania State University is currently investigating the concept for application in helicopter airframes.

1.2 Existing Research

In the past decade or so, the acoustic black hole effect has been studied by several research groups throughout the world including Loughborough University, University of Notre Dame, Laboratoire d'Acoustique de l'Université du Maine, Andreyev Acoustics Institute, and the Pennsylvania State University. Researchers divide their investigations of the ABH into a few general areas: one-dimensional, two-dimensional, and applications. Throughout the years, researchers explored each topic and received consistent results. They concluded that one-dimensional and two-dimensional ABHs efficiently dampen vibration energy even with very little viscoelastic damping material attached. Krylov[1] explains that the wave energy dissipation takes place mainly in a very small area near the thinnest part of the ABH. The key advantage of the ABH is that it requires a very small amount of damping material compared to traditional damping techniques. Further, Krylov claims that the results demonstrate that the "efficiency of vibration damping based on the acoustic black hole effect is substantially higher than that achieved by traditional methods." The weight and cost savings in addition to the efficiency gain make the ABH an incredible candidate to replace traditional vibration damping techniques on helicopter airframes.

A one-dimensional ABH takes an incident wave from one direction and focuses it toward the thinnest area of a wedge on the side of a plate. Mironov[2] first proposed the idea of using a plate with a sharp wedge to prevent wave reflection, drawn in Figure 2.

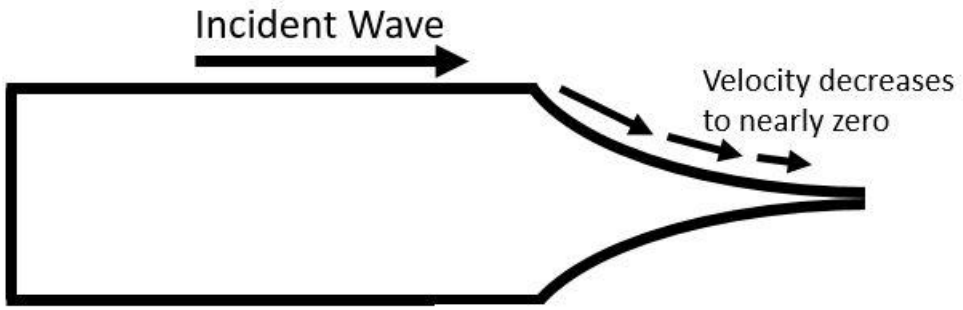

Figure 2. Cross-sectional diagram of the one-dimensional acoustic black hole.

Unfortunately, machine technology cannot create a perfectly straight and infinitely thin edge on the wedge, which hinders its performance as a vibration absorber. Additionally, an area of zero thickness would be detrimental to an aircraft's structural integrity. A research group at Loughborough University[3] investigated the effect of material deformation, and found that damage to the wedge tip does not destroy its performance benefits. To overcome the manufacturing difficulties, Bayod[4] investigated a case where they extended the sharp edge of the wedge. Results showed that this solution actually provided very efficient damping. The research group at Loughborough University[5] later proposed another solution where they machined the wedge inside the plate. This moved the exposed edge inside and created the appearance of a slot. They carried out various experiments with the slot, successfully achieving a maximum damping of 11 dB on a steel plate.

Another potential source of efficiency loss is attaching the wedge to the side of the plate via welding or gluing instead of using a homogeneous plate with a machined wedge on the side. The research group at Loughborough University[6] investigated this problem and found that these cases did not significantly decrease the vibration damping efficiency of the wedge. Although machining error can cause some efficiency loss, Krylov[1] claims that, "the acoustic black hole effect is robust enough and can be used widely without the need of high precision

manufacturing." Even so, investigations at Loughborough University revealed that wedge performance was improved by attaching damping material to the edge (Krylov[7]).

The research group at Loughborough University[8] applied the one-dimensional ABH effect with damping material to various plates and beams bounded by the wedges. Each experiment proved that the concept is much more efficient than traditional damping methods. Research at Loughborough University eventually led to the application of the power-law profile to the trailing edge of a turbofan blade (Krylov[1] and Winward[9]). Experimental investigation showed results that were consistent with earlier findings for the wedge on the side of a plate (Loughborough University[10]). The blade efficiently dissipated the vibration, proving that the acoustic black holes effect could help control vibration in engines.

As discussed above, the problem with one-dimensional acoustic black holes is the difficulty in machining the sharp power-law edge. To avoid this issue, Krylov[11] theoretically proposed the use of a tapered pit to trap bending waves, shown in Figure 3. This pit would take incident bending waves from any direction and slow them as they travel towards the center of the pit. The waves would slow so much that they would not reflect from the far side of the pit.

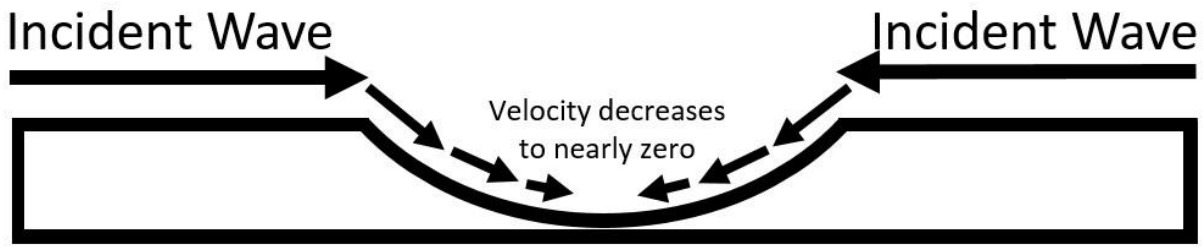

Figure 3. Cross-sectional diagram of the two-dimensional acoustic black hole.

Gautier[13] and his team carried out the first experimental investigation of the two-dimensional ABH in the case where all radiated bending waves were focused in the area of the pit. Results matched the theoretical predictions; the pit trapped the bending waves, and the

damping material in the center dissipated the vibration. Further experiments at Loughborough University[14] revealed that pits that are just protruding over the opposite plate surface do not effectively dissipate vibration. However, drilling a small hole through the center of the pit greatly increased the damping. Krylov[1] explains that the pits become curved power-law wedges, and therefore display similar damping characteristics as the one-dimensional wedges.

Next, researchers arranged a grid of pits on a plate to test if the damping efficiency would increase. Conlon[15] and his team at the Pennsylvania State University analyzed the low frequency performance of such plates since the reduction of these frequencies are important in many air vehicle applications. Experimental results showed that only the damping material reduced vibration at low frequencies, indicating that that the ABHs only dissipate vibration above a specific cut-on frequency. Vibration reduction increased as the incident wave frequency increased. In response to the experiments, Conlon claimed that at low frequencies the grid of pits acts as a resonant structure that researchers can tune to increase the overall vibration reduction of the system. He plans to explore tuning optimization by analyzing the effect of spacing, size, and other geometrical parameters of the ABH grid. Additionally, he plans to explore the structural integrity problems associated with its application in a real airframe.

Another significant area of research involves using composite materials for one-dimensional and two-dimensional ABHs. Composites inherently have a large vibration loss factor, enabling ABHs of this material to dissipate vibration while simultaneously decreasing the overall weight of air vehicles. Experimental investigations carried out at Loughborough University[16] showed that the composite material increased the damping efficiency of the ABHs and rid the need of additional damping material.

An extended application of the ABH is its use in harvesting vibration energy. In collaboration with the University of Notre Dame and Purdue University, Conlon[17] of the Pennsylvania State University created a piezoelectric-based energy harvesting system using a grid of two-dimensional ABH pits. Since two-dimensional ABH pits trap bending waves, they also localize the vibration energy of the plate to discrete areas. Instead of dissipating the vibration with damping material, one could theoretically harvest the energy by converting it to electrical energy. Experimental results showed that the grid of pits drastically increased the amount of energy harvested compared to that of a uniform plate without the grid.

1.3 Research Objectives

The following experiments will investigate the vibration reduction effectiveness of two-dimensional ABH grid treatments with particular interests in airframe applications. Broadband space averaged vibration response characteristics, along with the maximum and minimum variation about the mean, will be quantified for plates of varying degrees of vibration control and damping. Experiments will also explore the roles of the ABHs and of the damping layer. All of these topics are important considerations for aircraft designers who would like to incorporate ABH vibration control features into their designs. Future work will experimentally assess the vibration reduction capability of a novel "add-on" ABH single cell that could be attached to existing airframes.

Chapter 2

Procedure

2.1 Experimental Set-up and Data Acquisition

Under the guidance and supervision of Dr. Stephen C. Conlon and graduate student Philip A. Feurtado at the Pennsylvania State University, experimental tests explored the broadband vibration response of three aluminum plates with varying degree of vibration control and damping, whose specifications are given in Table 1.

Table 1. Specifications for each aluminum plate used in the experiment.

	Uniform Plate	Undamped ABH Plate	Damped ABH Plate
Material	2024 Al Alloy	2024 Al Alloy	2024 Al Alloy
Length (cm)	91	91	91
Width (cm)	61	61	61
Thickness (mm)	6.35	6.35	6.35
Degree of Vibration Control	No control	4 x 5 grid of ABH vibration control	4 x 5 grid of ABH vibration control
Degree of Vibration Energy Damping	No damping	No damping	3 mm viscoelastic damping material on ABH cells
Total Plate Mass (kg)	9.4	8.1	8.6

The reference case for the experiment was a plate of uniform thickness with no applied damping material. The second case explored the role of the ABH cells using a plate with a grid of two-dimensional ABHs (10 cm diameter) machined into it and with no applied damping material, as shown in Figure 4.

Figure 4. Grid of two-dimensional ABHs machined into an aluminum plate.

The power-law thickness profile (in meters) of each ABH cell is

$$Y = 4.582x^{2.2} + 5.08E\text{-}4 \; . \qquad (2)$$

The third case explored the role of the damping material in the ABH effect using a plate with the same grid of ABHs as the second case, but with the addition of 3 mm thick viscoelastic damping material, shown in Figure 5, covering the entire surface of each ABH cell.

Figure 5. Viscoelastic damping material used in the experiment.

Each plate was mounted in a steel box frame to ensure repeatable boundary conditions, as shown in Figure 6.

Figure 6. Uniform plate mounted in a steel frame with shakers attached by an impedance head.

A visual diagram of the signal flow for the experiment is shown in Figure 7. First, a Polytec PSV400 scanning laser Doppler vibrometer generated the broadband vibration signal and sent it to the Crown XTI 2000 amplifier, where it was amplified. The signal was then sent to a Wilcoxon F4 electrodynamic shaker and to the Impedance Matching Network (Model N7C), which drove the Wilcoxon F7 piezoelectric shaker. The signals passed through two multimeters before reaching the F4 and F7 shakers to measure the input current and voltage, respectively, and prevent the system from overloading. The F4 and F7 shakers drove the plates with band-limited white noise from 20 Hz to 20 kHz. A PCB 288D01 impedance head (mounted on a stinger) connected the shakers to a single drive point on each plate, shown in Figure 8, to measure the drive point force.

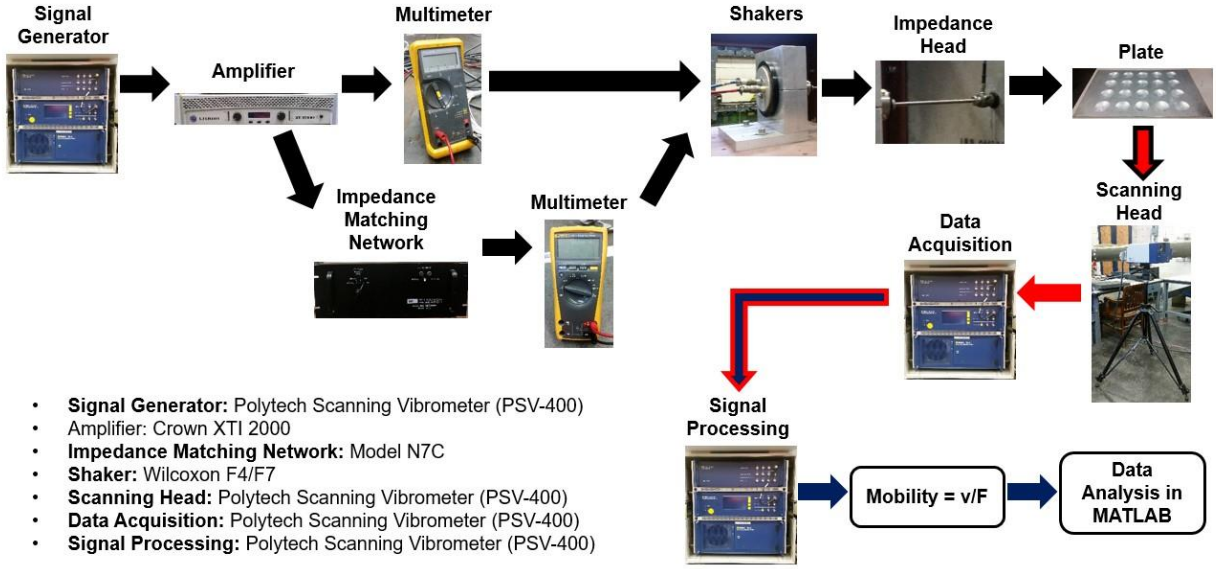

Figure 7. Visual signal flow diagram for the experiment.

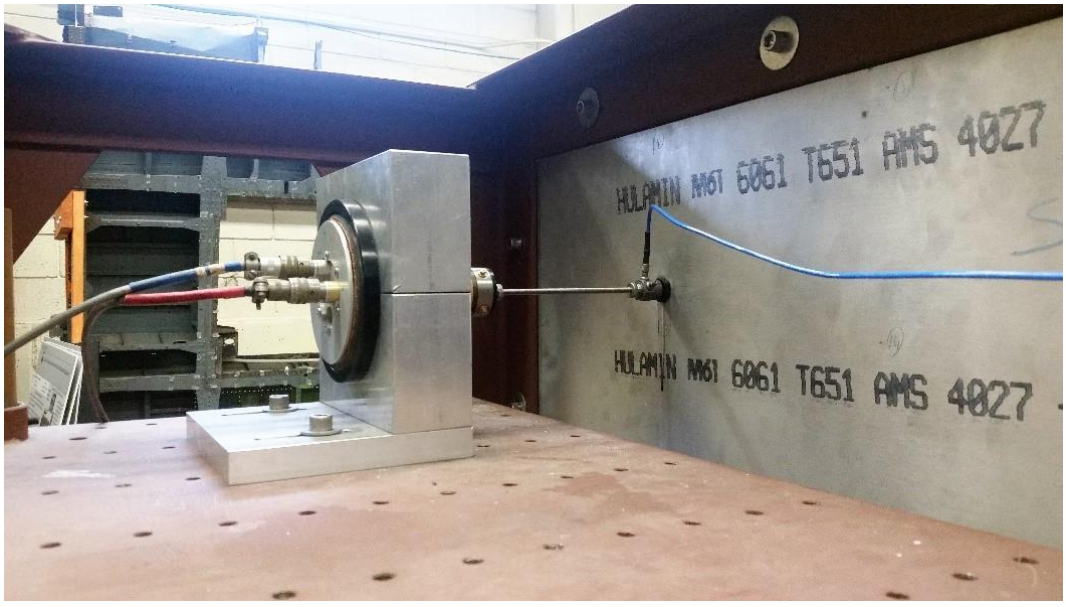

Figure 8. Wilcoxon shakers connected to a plate by an impedance head on a stinger.

The Polytec scanning laser Doppler vibrometer system used a laser to measure the plate velocity as a function of time at specific points across the plate, as shown in Figure 9.

Figure 9. Laser Doppler vibrometer scanning head pointing at a plate that is mounted on a steel frame.

The signal response of interest is the surface averaged mobility, defined as the surface velocity over the driving force (v / F). The Polytec system measured the complex mobility using Bendat's[21] method of

$$\hat{\mathrm{H}}_{f-v} = \frac{\hat{\mathrm{G}}_{fv}}{\hat{\mathrm{G}}_{ff}}, \tag{3}$$

where

$$\hat{\mathrm{G}}_{fv} = \frac{2}{T} E\{X_f^* X_v\} \tag{4}$$

is the force-velocity cross-spectrum,

$$\hat{\mathrm{G}}_{ff} = \frac{2}{T} E\{X_f^* X_f\} \tag{5}$$

is the force auto-spectrum, X_i is the Fourier Transform of the input, and the asterisk indicates the complex conjugate. The results were then analyzed in MATLAB (Appendix A). An overview of the signal flow is shown in Figure 10.

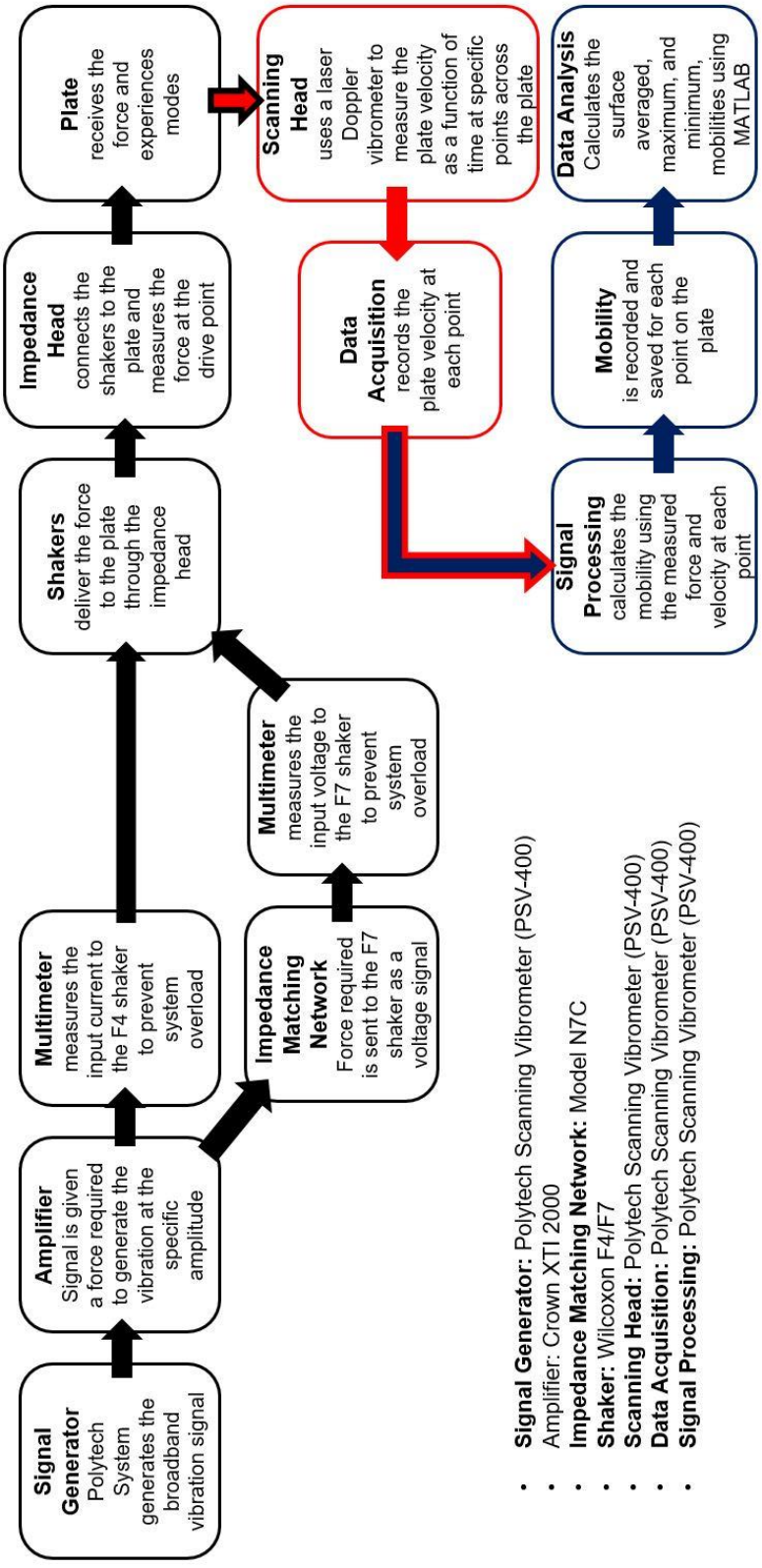

Figure 10. Overview of the signal flow for the experiment.

2.2 Infinite Plate Calibration

L. Cremer[20] mentions that the simple formulas used to describe infinite plates are equivalent to the mean vibration response at the drive point of a finite plate. To ensure that the signal response in this experiment was accurate, a calibration test compared the measured drive point mobility of the uniform finite plate to the theoretical mobility of an infinite uniform plate, described by

$$Y_c = \frac{1}{8\mu_s \kappa c_L}, \tag{6}$$

where

$$\mu_s = \rho * t = \text{surface mass density}, \tag{7}$$

$$\kappa = \sqrt{\frac{I}{A}} = \sqrt{\frac{(b*h^3)/12}{b*h}} = \frac{t}{2\sqrt{3}} = \text{cross section radius of gyration}, \tag{8}$$

$$c_L = \sqrt{\frac{E}{\rho(1-\nu^2)}} = \text{plate (quasi) longitudinal wave speed}, \tag{9}$$

ρ is the mass density, t is the plate thickness, E is the modulus of elasticity of 2024 Aluminum Alloy, and ν is Poisson's ratio. The theoretical mobility of an infinite plate is entirely real, while the mobility of a finite plate is complex. However as frequency increases, the drive point mobility approaches the theoretical infinite plate mobility from Equation 6. Therefore, the calibration compared only the real component of the drive point mobility to the infinite plate calculation.

To reduce measurement error, the calibration took into account the effect of the mass of the accelerometer and material of the impedance head in front of the force sensor using

$$Y_{measured\_mass\_corrected} = \frac{Y_{measured}}{1-(j\omega M)Y_{measured}}, \tag{10}$$

described by K.T. Brown[22] and P.R. Keswick[23], where $Y_{measured}$ is the experimentally measured drive point mobility, j is the imaginary unit vector, ω is the bending wave velocity given by

$$\omega = 2\pi f \ , \tag{11}$$

f is the frequency, and M is the mass between the impedance head and the plate.

Next, the calibration compared the mass corrected drive point mobility of the uniform plate to the theoretical mobility of the infinite plate. Figure 11 shows that the uniform plate mobility oscillates around a value close to the mobility of the infinite plate.

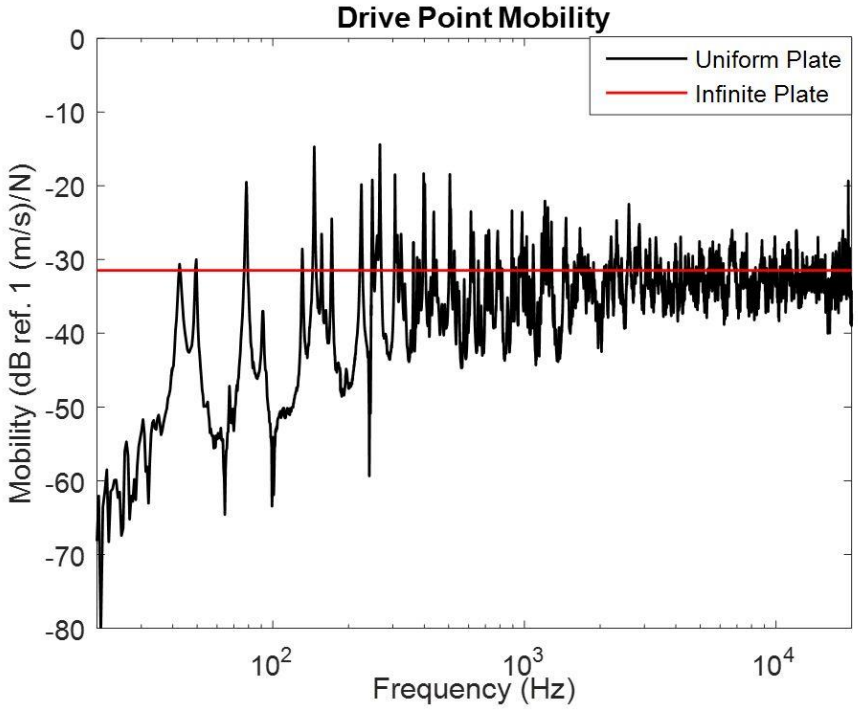

Figure 11. Mass corrected drive point mobility.

Although there is a small difference at low frequencies due to the drive point position towards a corner of the plates, Figure 11 confirms that the end-to-end calibrations are correct and that the experimental set up is ready for the planned series of experiments.

2.3 Data Processing

A Polytec PSV400 scanning laser vibrometer recorded the plate velocity as a function of time and spatial position and transformed it to mobility as a function of frequency and spatial position using force data from the impedance head. The mobility data was then processed using MATLAB (Appendix A). Previous researchers focused on analyzing the surface averaged mobility. This information gives great insight to the behavior of the plates, but does not tell the entire story. This experiment further analyzes the behavior by exploring the mobility variation about the mean, characterized by surface averaged, maximum, and minimum mobility measurements across each plate and across a single ABH cell. To do this, the code found the mean, maximum, and minimum values of the 273 spatial points on the plate and on the cell and converted this information into decibels (dB ref. 1 (m/s)/N), which is a common reference unit to acousticians. Finally, the code compared the surface averaged, maximum, and minimum mobility values of each plate and of the cell for frequencies from 20 Hz to 20 kHz.

Chapter 3

Results

3.1 Introduction

In general, the plates showed three patterns across the frequency range, divided by purple lines in Figure 12.

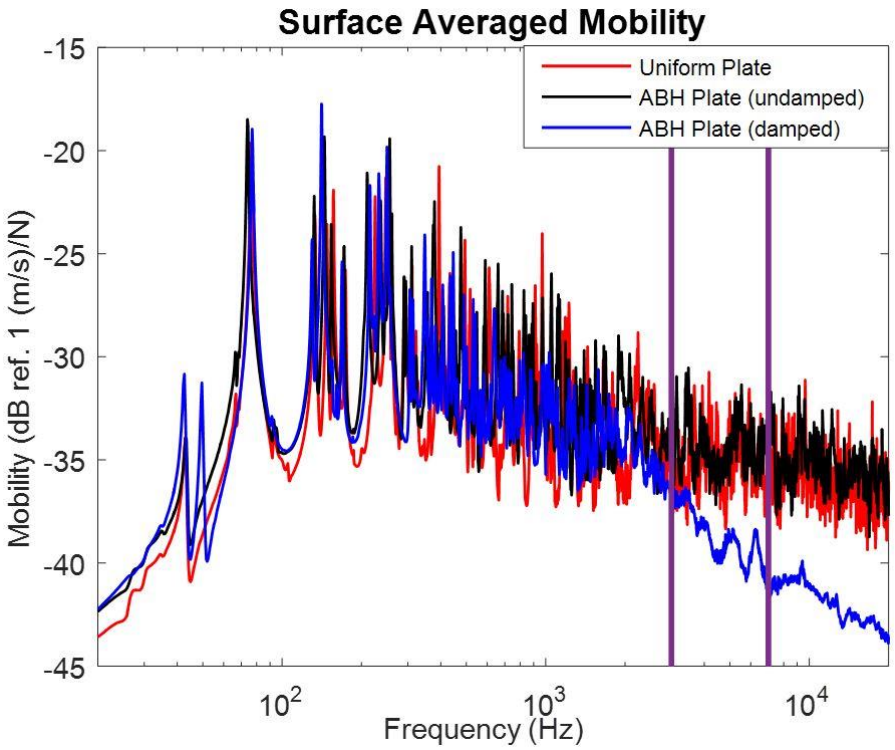

Figure 12. Surface averaged mobility of the plates for all frequency ranges. Purple lines separate the frequency ranges.

There is a distinct change in vibration response around 3 kHz where the ABHs begin to take effect. Prior to 3 kHz, only structure (plate coupled to fixture / frame) and plate modes influence the vibration response. The structural and plate mode shapes cut on around 40 Hz and 76 Hz, respectively. The frequency range from 20 Hz to 3 kHz is the low-frequency range. Between 3 kHz and 7 kHz, the effect of the damping material on the ABHs is a strong negative slope with

data that oscillates about the trend line. This is the mid-frequency range. Around 7 kHz, the effect of the damping material on the ABHs is a slightly weaker negative slope with data that follows more closely to the trend line. The frequency range from 7 kHz to 20 kHz is the high-frequency range. Figure 12 shows the comparison between the surface averaged mobilities of each plate at the three frequency ranges.

As mentioned in section 2.3, the experiment compares the surface averaged, maximum, and minimum mobilities for all three plates at each frequency range. The upper bound is the difference between the maximum and surface averaged mobilities in dB (ref. 1 (m/s)/N), while the lower bound is the difference between the surface averaged and minimum mobilities. The range is the difference between the maximum and minimum mobilities.

3.2 Low-Frequency

Only the structure and plate modes influence the vibration response in the low-frequency range. Although geometry and mass differences affect the vibration responses, the surface averaged mobilities of each plate are very similar in this range, shown by Figure 13.

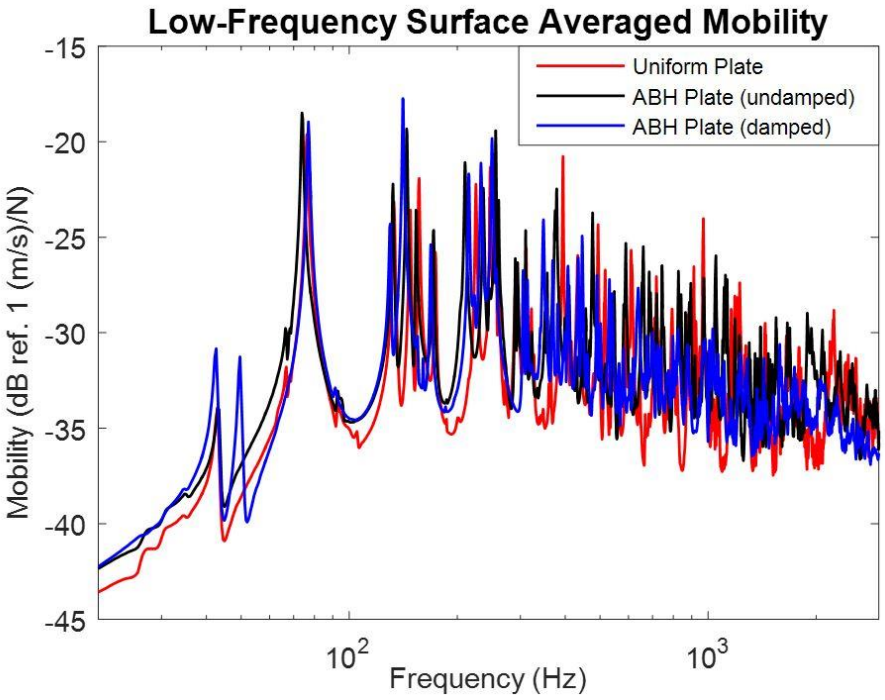

Figure 13. Low-frequency surface averaged mobility of the plates.

The uniform plate experienced the smallest surface averaged mobility, followed by the two plates with ABH grids. The maximum and minimum variation about the surface averaged mobility showed similar results, shown in Figures 14, 15, and 16, which display the surface averaged, maximum, and minimum mobilities of the uniform plate, undamped ABH plate, and damped ABH plate in the low-frequency range.

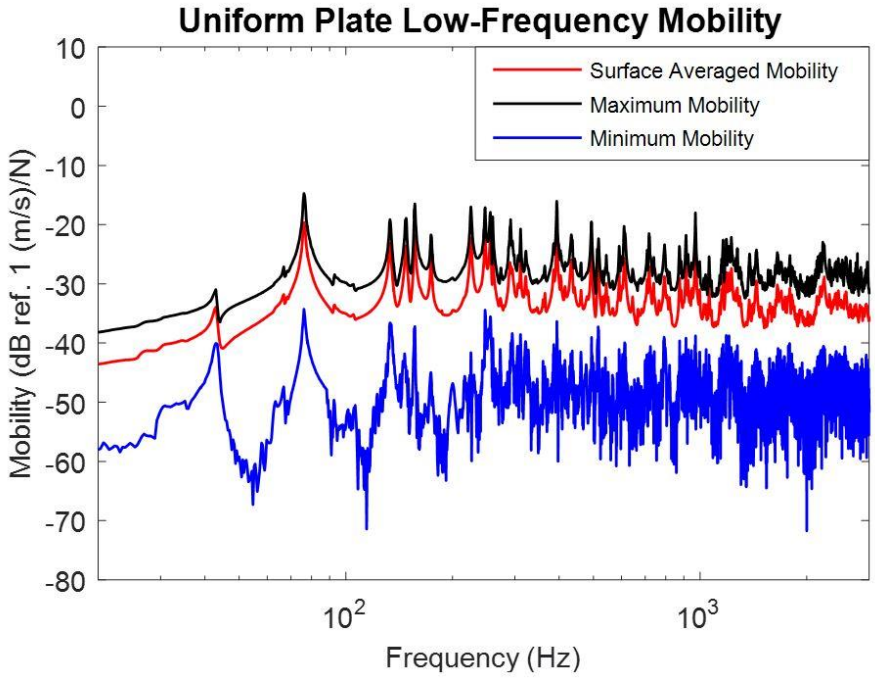

Figure 14. Surface averaged, maximum, and minimum mobilities of the uniform plate in the low-frequency range.

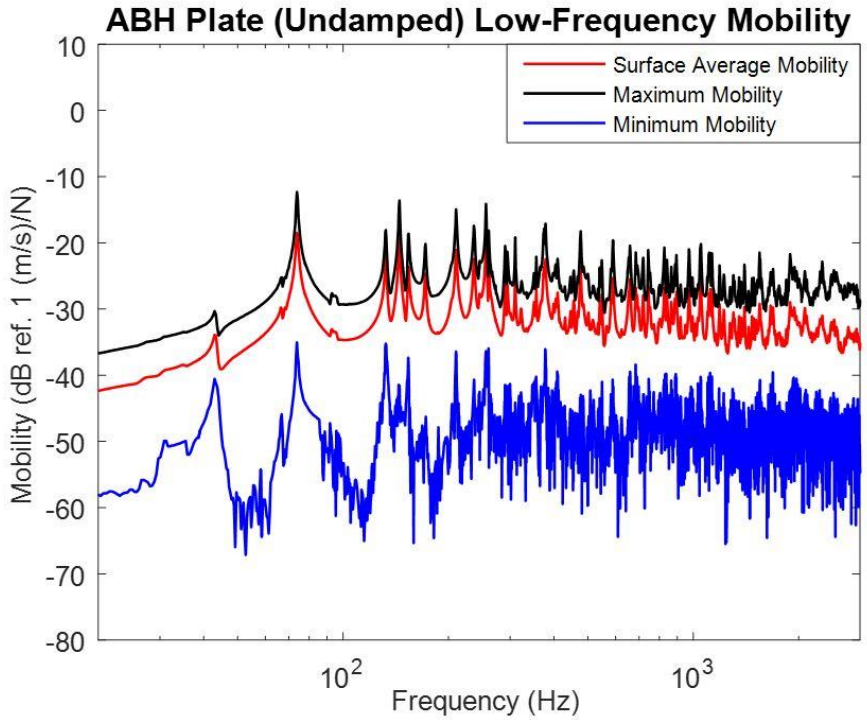

Figure 15. Surface averaged, maximum, and minimum mobilities of the undamped ABH plate in the low-frequency range.

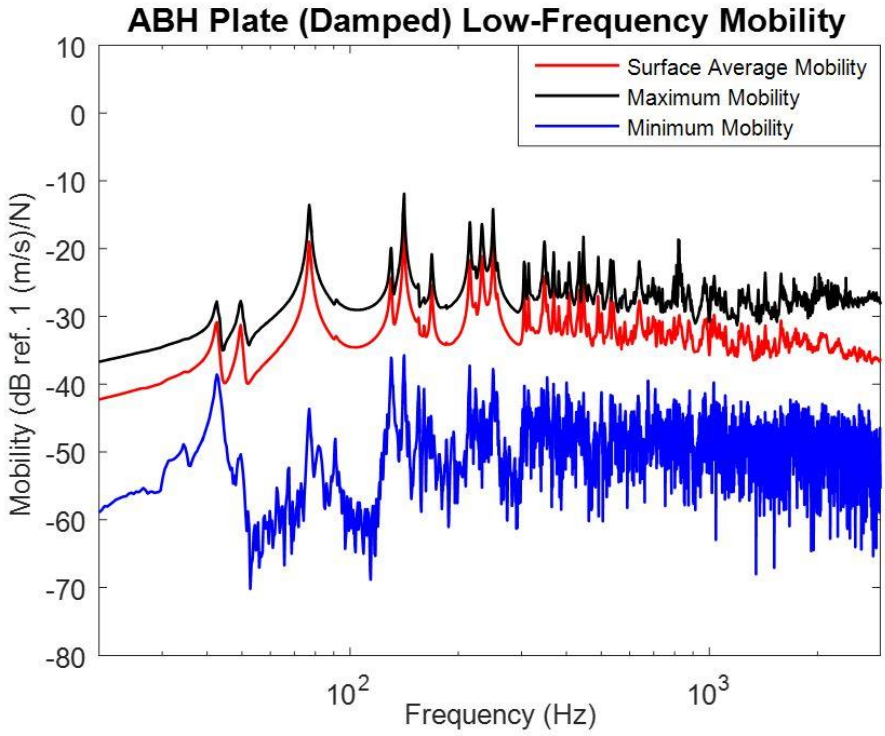

Figure 16. Surface averaged, maximum, and minimum mobilities of the damped ABH plate in the low-frequency range.

The upper and lower bounds of each plate in the low frequency range were calculated by taking the difference between the peak values of the surfaced averaged, maximum, and minimum mobility plots. Table 2 shows the results for each plate.

Table 2. Low-Frequency Mobility Comparison in dB of the plates.

	Uniform Plate	ABH Plate (undamped)	ABH Plate (damped)
Upper Bound	4.7	5.4	5.7
Lower Bound	15.9	16.5	18.2
Range	20.6	21.9	23.9

The upper bounds, lower bounds, and ranges were very similar between all three plates. The uniform plate experienced slightly less variation than the ABH plates, followed by the ABH plate without damping and then the ABH plate with damping. Mass and geometry differences

between the plates could explain the slight differences in the plates' vibration responses, since the global plate modes dominate the responses in the low frequency range.

3.3 Mid-Frequency

The surface averaged mobilities of the plates in the mid-frequency range were generally less than those in the low-frequency range. The uniform plate and the undamped ABH plate had the greatest mobilities, followed by the damped ABH plate, as displayed in Figure 17.

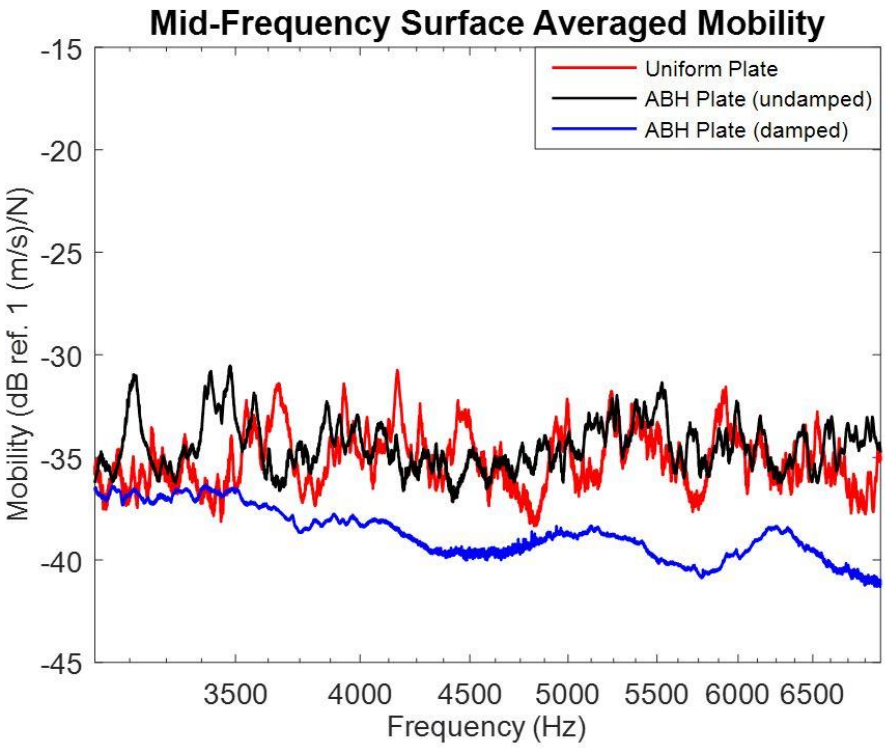

Figure 17. Mid-frequency surface averaged mobility of the plates.

The variation of responses between the plates was much greater than that of the low-frequency range because of the cut-on of the ABH modes. The damped ABH plate experienced a much lower mobility than the plates because of the damping material; the damping material dissipates much of the vibration energy since it is now focused in the ABH cells.

Figures 18, 19, and 20 show the maximum, minimum, and surface averaged mobility for the uniform plate, undamped ABH plate, and damped ABH plate.

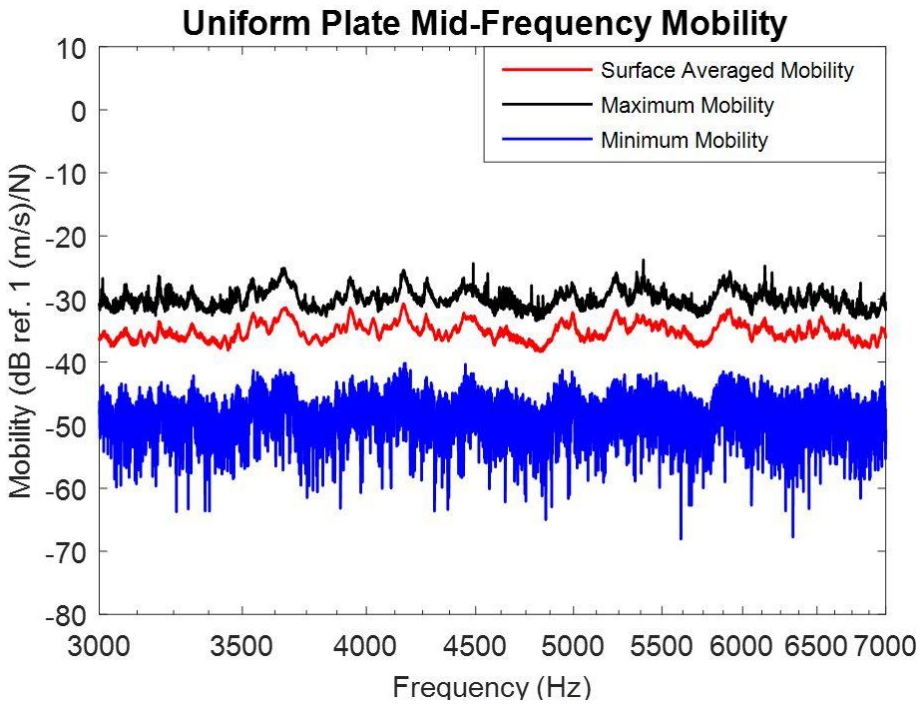

Figure 18. Surface averaged, maximum, and minimum mobilities of the uniform plate in the mid-frequency range.

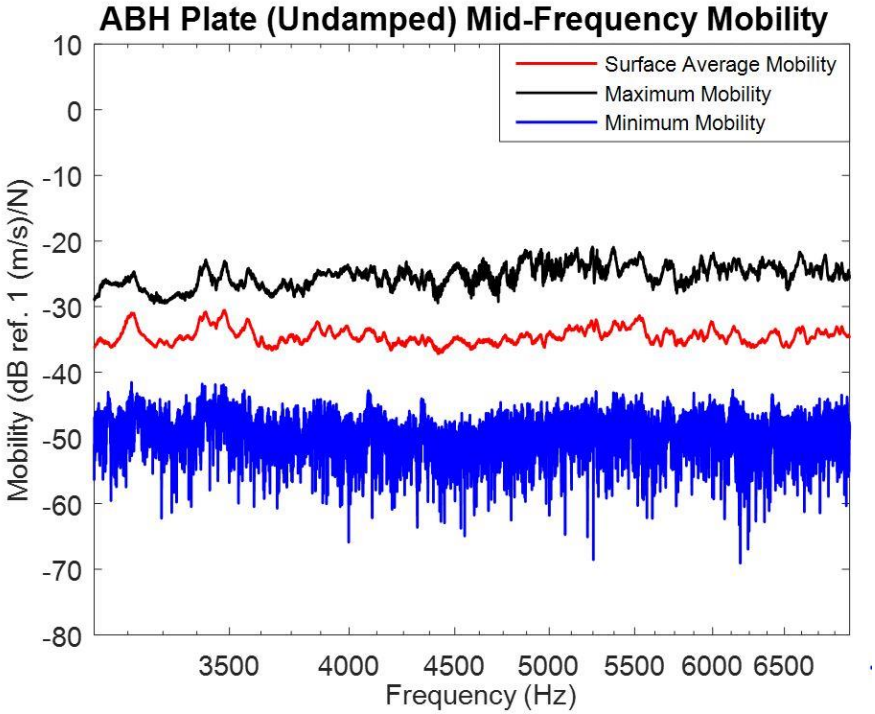

Figure 19. Surface averaged, maximum, and minimum mobilities of the undamped ABH plate in the mid-frequency range.

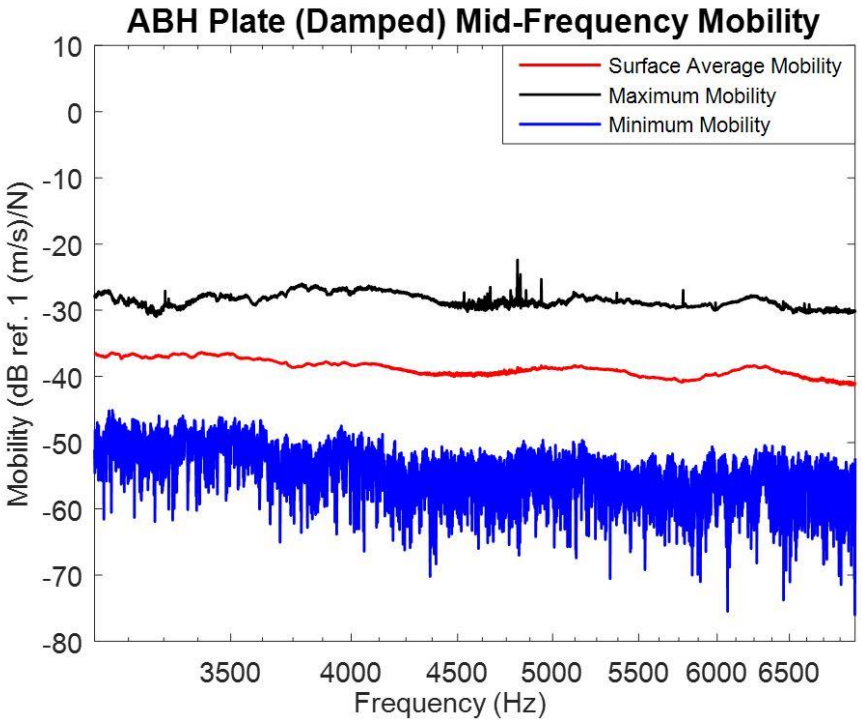

Figure 20. Surface averaged, maximum, and minimum mobilities of the damped ABH plate in the mid-frequency range.

The upper and lower bounds at the mid-frequency range were determined by first taking the average (over the frequency range) of the maximum surface mobilities, the average of the mean surface mobilities, and the upper limit of the minimum mobilities. Next, the upper bound, lower bound, and the range were calculated. Table 3 displays the results for the plates.

Table 3. Mid-Frequency Mobility Comparison in dB of the plates.

	Uniform Plate	ABH Plate (undamped)	ABH Plate (damped)
Upper Bound	6.6	9.3	7.2
Lower Bound	9.3	12.2	6.2
Range	15.9	21.5	13.4

The undamped ABH plate had much larger upper and lower bounds than the other two plates because of the focusing of vibration energy in the ABHs. As the cross-sectional mass of the plate decreases in the ABH, the surface velocity increases to conserve vibrational energy. Therefore, although the mobilities of the uniform plate and the undamped ABH plate are similar, the bounds are different because the vibrational energy of the undamped ABH plate is focused to the ABHs, and there is no damping material to dissipate the energy. The damped ABH plate experiences a significant decrease in bounds because the damping material dissipates much of the vibrational energy of the plate.

3.4 High-Frequency

The surface averaged mobility in the high-frequency range experienced a similar pattern that that of the mid-frequency range, shown in Figure 21.

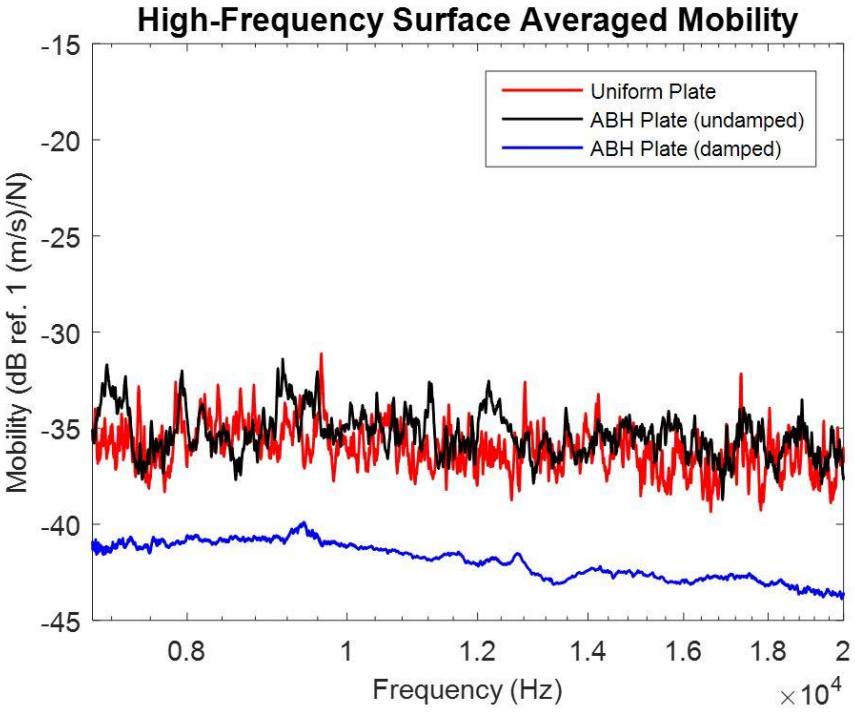

Figure 21. High-frequency surface averaged mobility of the plates.

The mobilities of the uniform plate and the undamped ABH plate remain approximately constant with only slight decreases in magnitude. The damped ABH experiences a steady decrease in mobility from the ABH effect, with a slightly less negative slope than that of the mid-frequency range. The damped ABH plate mean mobility is approximately 6 to 8 dB below the uniform plate even though it is lighter, shown in Table 1. Each plate experienced very different maximum, minimum, and surface averaged responses, shown in Figures 22, 23, and 24.

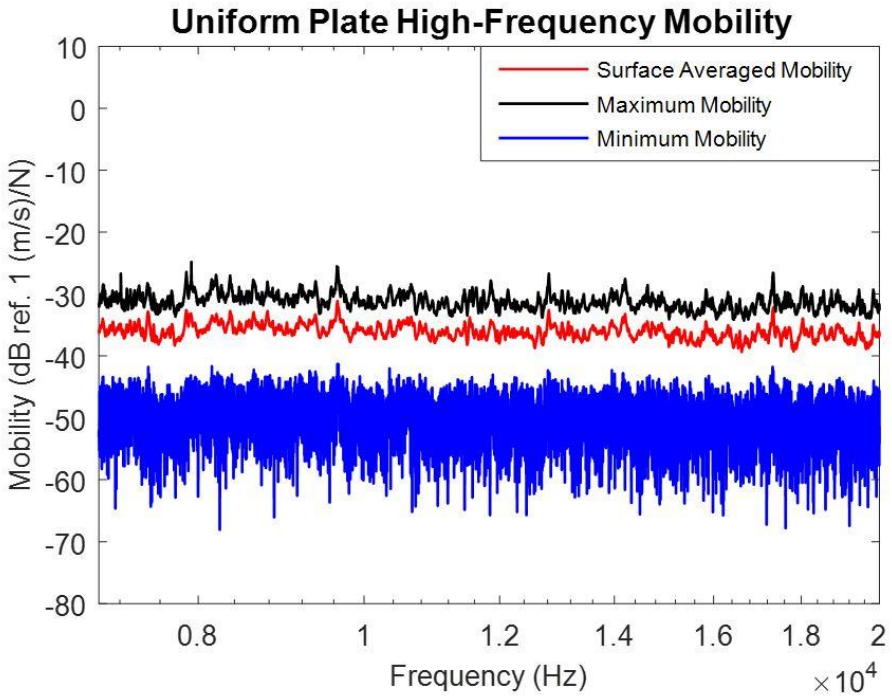

Figure 22. Surface averaged, maximum, and minimum mobilities of the uniform plate in the high-frequency range.

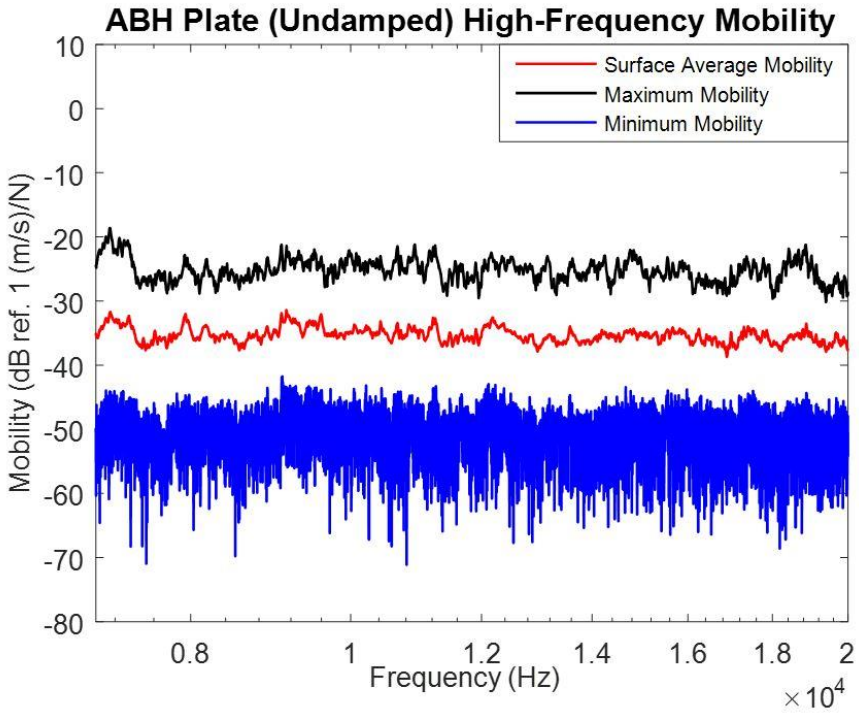

Figure 23. Surface averaged, maximum, and minimum mobilities of the undamped ABH plate in the high-frequency range.

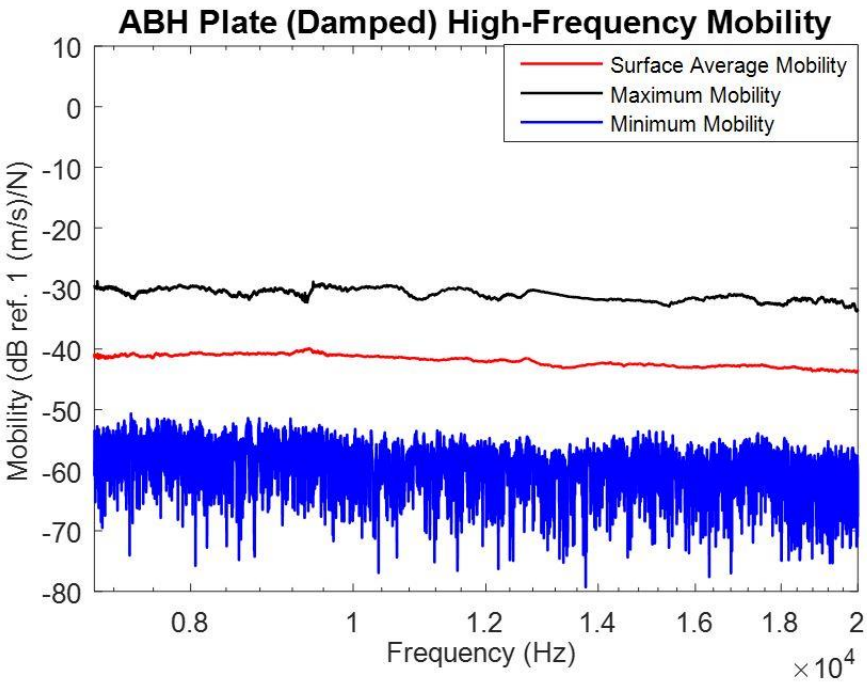

Figure 24. Surface averaged, maximum, minimum mobilities of the damped ABH plate in the high-frequency range.

The uniform plate and the undamped ABH plate experienced oscillatory responses for the maximum, minimum, and surface averaged mobilities. The oscillations were closer together for the uniform plate, while the oscillations for the undamped ABH plate had greater amplitude. The damped ABH plate experienced smooth responses because of the damping material.

The bounds were calculated using the same method described for the mid-frequency range. Table 4 shows the results for the plates.

Table 4. High-Frequency Mobility Comparison in dB of the plates.

	Uniform Plate	ABH Plate (undamped)	ABH Plate (damped)
Upper Bound	5.2	9.9	6.8
Lower Bound	9.2	11.3	6.2
Range	14.4	21.2	13.0

The high-frequency impact of the ABH effect led to a slight decrease in bounds. Similar to the mid-frequency results, the undamped ABH plate had much larger upper and lower bounds than the other two plates because of the vibration energy is focused in the ABHs. The damped ABH plate experiences a constant decrease in surface averaged mobility, but the bounds only change slightly.

3.5 ABH Cell

A detailed scan of an ABH cell located in the top right position of the undamped ABH plate, shown in Figures 25 and 26, revealed the characteristics of the ABH at all three frequency ranges, shown in Figure 27.

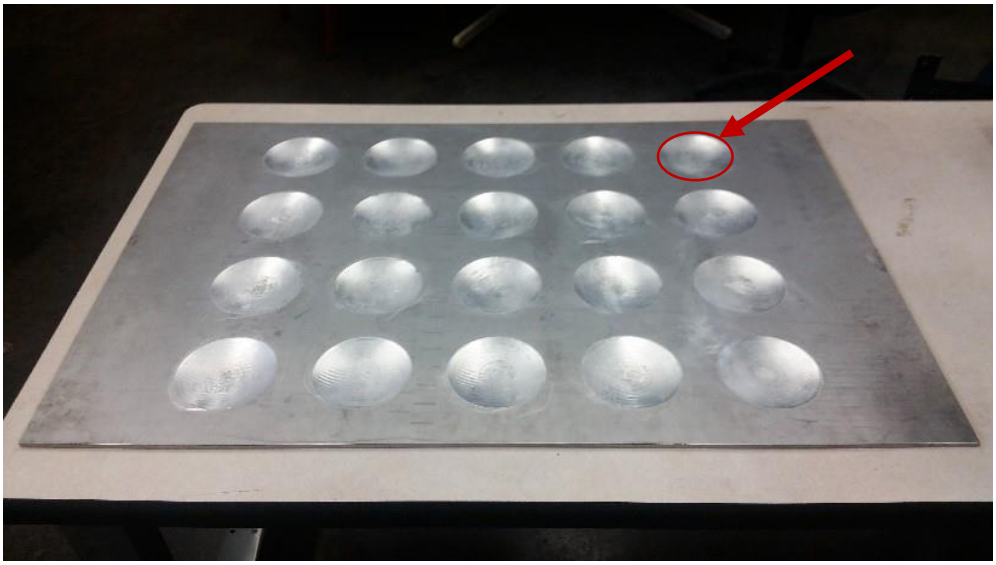

Figure 25. Position of the ABH cell used in the detailed scan.

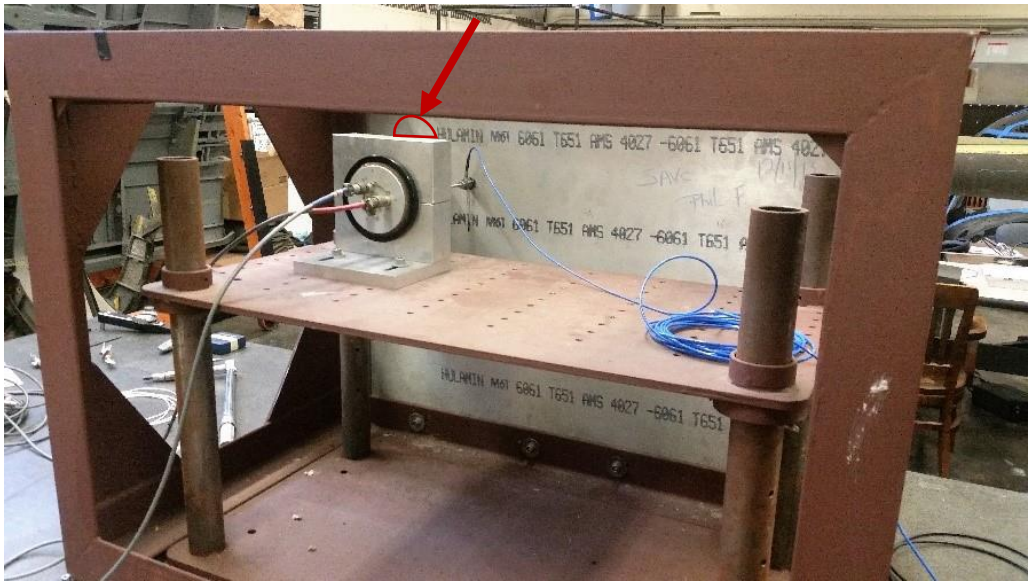

Figure 26. Position of the ABH cell used in the detailed scan relative to the position of the impedance head.

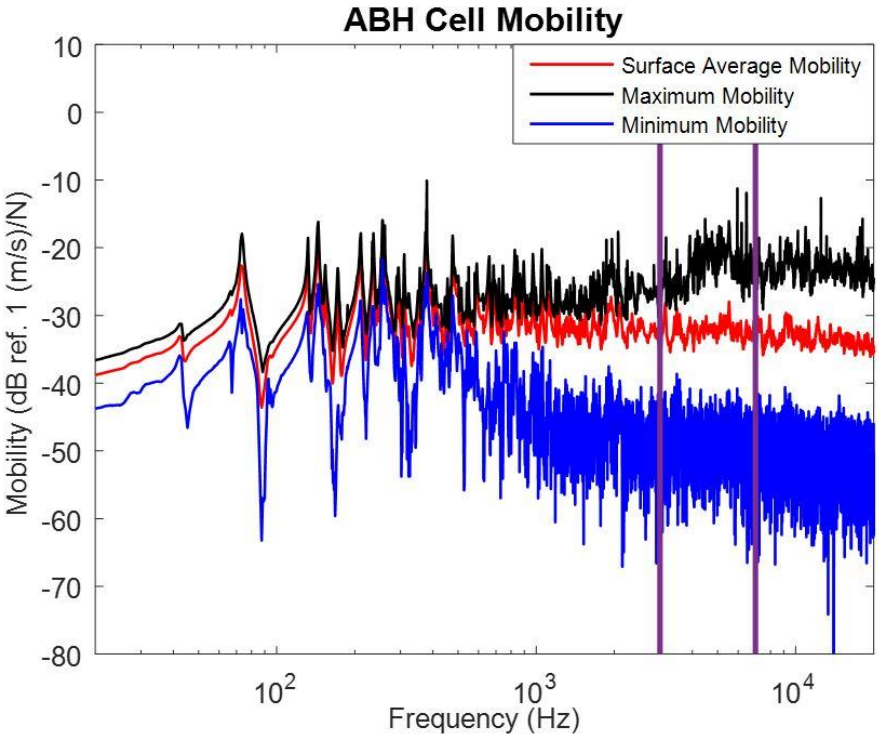

Figure 27. Surface averaged, maximum, and minimum mobilities of the ABH cell.

At the low frequency range, the cell mobility followed a similar pattern to that of the plates, but was generally about 1 dB larger. The cell experienced a similar upper bound, but a much smaller

lower bound than the plates. Possible error induced by the geometric location of the ABH cell on the plate could explain the difference in lower bound. The surface averaged mobility of an ABH cell positioned on a node would be very difference than the mobility of one positioned in the center of the plate.

The surface averaged mobility of the ABH cell was greater than that of the plates in the mid-frequency range. This is because the average consisted of only the ABH, whereas the averages of the plates included the areas outside of the ABHs (areas of constant thickness). The The bounds and range of the ABH cell at the mid-frequency range increases drastically as the frequency increases past 3 kHz. They are higher than those of the uniform plate and the damped ABH plate due to the focusing of vibration energy in the ABH cell.

At the high-frequency range, the surface averaged mobility remains approximately constant and is greater than that of all of the plates. Since the plate is excited above the cut-on frequency, the ABH effect has a drastic impact on the mobility of the cell. However, past 7 kHz the bounds and range become practically constant. Similar to the mid-frequency results, the ABH cell had much larger upper and lower bounds than the other two plates because the vibration energy is focused on the ABH cell, which increases the mobility. A summary of results for each frequency range is in Table 5.

Table 5. Comparison of all upper bounds, lower bounds, and ranges in dB.

	Uniform Plate	ABH Plate (undamped)	ABH Plate (damped)	ABH Cell
Low-Frequency				
Upper Bound (dB)	4.7	5.4	5.7	5.8
Lower Bound (dB)	15.9	16.5	18.2	6.9
Range (dB)	20.6	21.9	23.9	11.4
Mid-Frequency				
Upper Bound (dB)	6.6	9.3	7.2	8.5
Lower Bound (dB)	9.3	12.2	6.2	12.6
Range (dB)	15.9	21.5	13.4	21.1
High-Frequency				
Upper Bound (dB)	5.2	9.9	6.8	9.3
Lower Bound (dB)	9.2	11.3	6.2	12.3
Range (dB)	14.4	21.2	13.0	21.6

Chapter 4

Conclusions

The experimental results showed that the ABH successfully focuses vibration energy from the plate to the center of the two-dimensional cell and that the added layer of damping material effectively reduces the vibrational energy of the structure.

The low-frequency responses were very similar amongst all three plates, as expected, since global modes in the plate dominate the response. Slight differences could be explained by geometric and mass differences between the plates. The mid-frequency responses, after the cut-on of the ABH cells, displayed significant differences for each plate. The undamped ABH plate and the uniform plate showed similar results, although the undamped ABH plate had much higher upper and lower bounds, explained by the focusing of energy and thus higher response amplitudes in the ABH cells. The damped ABH plate experienced a decrease in surface averaged mobility and decreases in upper and lower bounds because of the added layer of damping material, allowing for an enhanced damping mechanism. The ABH cells effectively focus and trap the energy where it can then be dissipated in the damping layers. The high-frequency surface averaged mobilities were similar to the mid-frequency responses, although much smoother due to even higher levels of effective damping, shown by a general decrease in maximum / minimum variation about the surface averaged mobility.

The ABH cell measurements showed differences as compared to the plate space averaged measurements. In the low-frequency range, the differences were probably due to as bias because of the measured ABH cell geometric position on the plate. The upper bounds, lower bounds, and ranges in the mid-frequency and high-frequency ranges of the ABH cell mobility were very similar to those of the undamped ABH plate due to the (undamped) focusing of vibration energy

to the center of the ABHs. The ABH cell experienced slightly larger values because the average consisted of only the ABH, whereas the average for the undamped ABH plate included the areas outside of the ABHs.

The results of this experiment are important because they show that the ABH treatment drastically reduces the vibration energy response of a structure due to a point force excitation, while adding very little weight. With further development, this idea will give design engineers an alternative to traditional heavy and inefficient acoustic treatments. If applied to aircraft, the ABH has the potential to significantly decrease the weight devoted to acoustic treatments, enabling possible increases in fuel efficiency.

One potential problem with the application of embedded ABH cells is that they could compromise structural rigidity. A possible solution that would not compromise structural rigidity is an add-on component. This concept is under development and uses the same ABH features as the two-dimensional ABH, but could be attached to an existing airframe. An experimental model of such a device is shown in Figure 28.

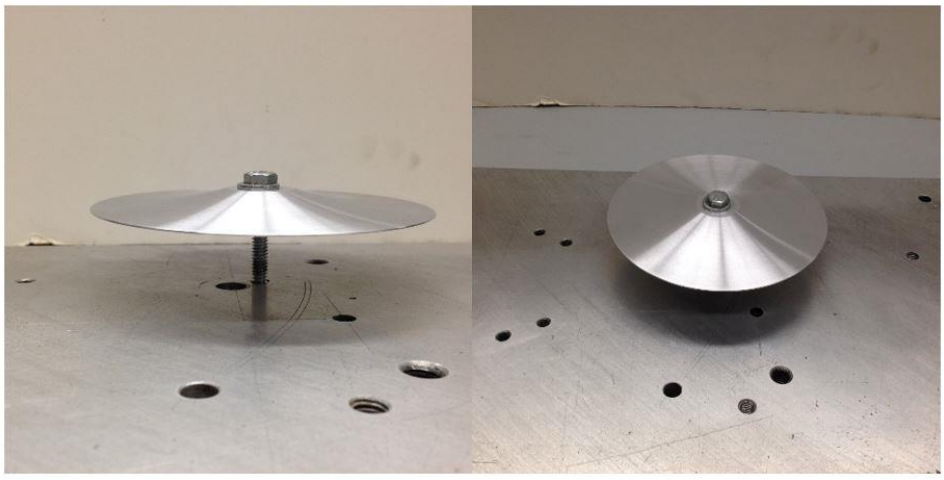

Figure 28. Two-dimensional ABH add-on device that could be bolted into existing airframes.

Future work will focus on testing the vibration response and efficiency of this add-on device.

Appendix A

MATLAB Code used for Data Analysis

```
% Surface Averaged Mobility
% Takes the surface averaged mobility of the plates.

close all
clc

% Load files
load flat_plate_mobility.mat;
load mobility_abh_plate_angelina.mat;
load mobility_10cm_damping.mat;
load freqs.mat;

% Renames the mobility matrix and takes the absolute value
mobility_fp = abs(mobilty_flat_plate);
mobility_abh = abs(mobilty_abh_plate);
mobility_abh_damp = abs(mobility_10cm_matrix);

% Takes the mean, max, and min of the mobility matrix
sa_mobility_fp = mean(mobility_fp, 2);
max_mobility_fp = max(mobility_fp,[],2);
min_mobility_fp = min(mobility_fp,[],2);

sa_mobility_abh = mean(mobility_abh, 2);
max_mobility_abh = max(mobility_abh,[],2);
min_mobility_abh = min(mobility_abh,[],2);

sa_mobility_abh_damp = mean(mobility_abh_damp, 2);
max_mobility_abh_damp = max(mobility_abh_damp,[],2);
min_mobility_abh_damp = min(mobility_abh_damp,[],2);

% Converts units to dB
sa_mobility_dB_fp = 10*log10(sa_mobility_fp);
max_mobility_dB_fp = 10*log10(max_mobility_fp);
min_mobility_dB_fp = 10*log10(min_mobility_fp);

sa_mobility_dB_abh = 10*log10(sa_mobility_abh);
max_mobility_dB_abh = 10*log10(max_mobility_abh);
min_mobility_dB_abh = 10*log10(min_mobility_abh);

sa_mobility_dB_abh_damp = 10*log10(sa_mobility_abh_damp);
max_mobility_dB_abh_damp = 10*log10(max_mobility_abh_damp);
```

```
min_mobility_dB_abh_damp = 10*log10(min_mobility_abh_damp);

% Creates lines to show the frequency bounds
lower_bound = 3000;
upper_bound = 7000;

% Plots Uniform Plate surface averaged, maximum, and minimum
mobilities
figure
plot(freqs, sa_mobility_dB_fp)

hold on
plot(freqs, max_mobility_dB_fp)
plot(freqs, min_mobility_dB_fp)
plot([lower_bound lower_bound], [0 -80])
plot([upper_bound upper_bound], [0 -80])
hold off

title('Uniform Plate Mobility');
xlabel('Frequency (Hz)');
ylabel('Mobility (dB ref. 1 (m/s)/N)');
legend('Surface Average Mobility', 'Maximum Mobility', 'Minimum
Mobility');

% Plots undamped ABH Plate surface averaged, maximum, and minimum
mobilities
figure
plot(freqs, sa_mobility_dB_abh)

hold on
plot(freqs, max_mobility_dB_abh)
plot(freqs, min_mobility_dB_abh)
plot([lower_bound lower_bound], [0 -80])
plot([upper_bound upper_bound], [0 -80])
hold off

title('ABH Plate (Undamped) Mobility');
xlabel('Frequency (Hz)');
ylabel('Mobility (dB ref. 1 (m/s)/N)');
legend('Surface Average Mobility', 'Maximum Mobility', 'Minimum
Mobility');

% Plots the damped ABH Plate surface averaged, maximum, and minimum
mobilities
figure
plot(freqs, sa_mobility_dB_abh_damp)

hold on
plot(freqs, max_mobility_dB_abh_damp)
plot(freqs, min_mobility_dB_abh_damp)
```

```
plot([lower_bound lower_bound], [0 -80])
plot([upper_bound upper_bound], [0 -80])
hold off

title('ABH Plate (Damped) Mobility');
xlabel('Frequency (Hz)');
ylabel('Mobility (dB ref. 1 (m/s)/N)');
legend('Surface Average Mobility', 'Maximum Mobility', 'Minimum
Mobility');

% Plots the surface averaged mobilities for all plates
figure
plot(freqs, sa_mobility_dB_fp)

hold on
plot(freqs, sa_mobility_dB_abh)
plot(freqs, sa_mobility_dB_abh_damp)
plot([lower_bound lower_bound], [0 -80])
plot([upper_bound upper_bound], [0 -80])
hold off

title('Surface Averaged Mobility');
xlabel('Frequency (Hz)');
ylabel('Mobility (dB ref. 1 (m/s)/N)');
legend('Uniform Plate', 'ABH Plate (undamped)', 'ABH Plate (damped)');

%%
% Takes the surface averaged, maximum, and minimum mobilities of the
% ABH Cell.

close all
clc

% Load file
load ABH_element_mobility;

% Renames the mobility matrix and takes the absolute value
mobility_cell = abs(mobilty);

% Takes the mean, max, and min of the mobility matrix
sa_mobility_cell = mean(mobility_cell, 2);
max_mobility_cell = max(mobility_cell,[],2);
min_mobility_cell = min(mobility_cell,[],2);

% Converts units to dB
sa_mobility_dB_cell = 10*log10(sa_mobility_cell);
max_mobility_dB_cell = 10*log10(max_mobility_cell);
min_mobility_dB_cell = 10*log10(min_mobility_cell);

% Creates lines to show the frequency bounds
```

```
lower_bound = 3000;
upper_bound = 7000;

% Plots ABH Cell surface averaged, maximum, and minimum mobilities
figure
plot(freqs, sa_mobility_dB_cell)

hold on
plot(freqs, max_mobility_dB_cell)
plot(freqs, min_mobility_dB_cell)
plot([lower_bound lower_bound], [0 -80])
plot([upper_bound upper_bound], [0 -80])
hold off

title('ABH Cell Mobility');
xlabel('Frequency (Hz)');
ylabel('Mobility (dB ref. 1 (m/s)/N)');
legend('Surface Average Mobility', 'Maximum Mobility', 'Minimum
Mobility');

%%
% Finds the mass-corrected drive point mobility

close all
clc

% Loads files
load uniform_plate_drive_point.mat;
load freqs.mat;

% Defines important variables
omega = 2 .* pi .* freqs';
M = 20 * 10^-3; %mass in kg
t = 0.00635; %thickness in meters
k = t/(2*sqrt(3)); %cross section radius of gyration
E = 6894.76 * 1.05e7; %modulus of elasticity of 2024 Al Alloy in Pa
rho = 27679.8 * 0.101; %density in kg/m^3
nu = 0.33; %Poisson's ratio
CL = sqrt(E/(rho*(1-(nu^2)))); %plate (quasi) longitudinal wave speed
mu = rho * t; %surface mass density in kg/m^2

% Mass Correction to Drive Point Mobility
fp_mc = drv_pnt_mob ./ ( 1 - ( 1i * omega * M ) .* drv_pnt_mob);

% Takes the real part of the drive point mobility and convert to dB
fp_realmobility = real(fp_mc);
fp_realmobility_dB = 10*log10(fp_realmobility);

% Calculates the mobility of a uniform infinite plate and converts it
% to dB
```

```
Yinf = 1 / (8*mu*k*CL);
Yinf_dB = 10*log10(Yinf);

% Plots the Mass Corrected Drive Point Mobility of the Uniform Finite
Plate and the Mobility of a Uniform Infinite Plate
figure
plot(freqs, fp_realmobility_dB)

hold on
plot([1 20000], [Yinf_dB Yinf_dB])
hold off

title('Drive Point Mobility');
xlabel('Frequency (Hz)');
ylabel('Mobility (dB ref. 1 (m/s)/N)');
legend('Uniform Plate', 'Infinite Plate');

%%
% Plots the bands of the plates

%Band Data
data_freq_range = [1, 2, 3];
flat_plate = [20.6, 15.9, 14.4];
abh_plate = [21.9, 21.5, 21.2];
abh_damp_plate = [23.9, 13.4, 13];

%Plot
figure
plot(data_freq_range, flat_plate)

hold on
plot(data_freq_range, abh_plate)
plot(data_freq_range, abh_damp_plate)
hold off

title('Plate Mobility Variation');
xlabel('Frequency Range');
ylabel('Mobility Variation (dB ref. 1 (m/s)/N)');
legend('Uniform Plate', 'ABH Plate (undamped)', 'ABH Plate (damped)');
```

REFERENCES

1. V. V. Krylov, *Acoustic black holes and their applications for vibration damping and sound absorption*, in: *Proceedings of ISMA2012-USD2012*, pp. 933-942.
2. M. A. Mironov, *Propagation of a flexural wave in a plate whose thickness decreases smoothly to zero in a finite interval*, in: Soviet physics. Acoustics, Vol. 34(3) (1988), pp.318-319.
3. E. P. Bowyer, D.J. O'Boy, V.V. Krylov, J.L. Horner, *Effect of geometrical and material imperfections on damping flexural vibrations in plates with attached wedges of power law profile,* Applied Acoustics, Vol. 73 (2012), pp. 514-523.
4. J. J. Bayod, *Experimental study of vibration damping in a modified elastic wedge of power-law profile,* Journal of Vibration and Acoustics, Vol. 133 (2011), 061003.
5. E. P. Bowyer, V.V. Krylov, D.J. O'Boy, *Damping of flexural vibrations in rectangular plates by slots of power-law profile*, in: Proceedings of the conference 'Acoustics 2012', Nantes, France, 2327 April 2012, pp. 2187-2192.
6. E. P. Bowyer, D.J. O'Boy, V.V. Krylov, J.L. Horner, *Effect of geometrical and material imperfections on damping flexural vibrations in plates with attached wedges of power law profile,* Applied Acoustics, Vol. 73 (2012), pp. 514-523.
7. V. V. Krylov, *Laminated plates of variable thickness as effective absorbers for flexural vibrations*, in: Proceedings of the 17th International Congress on Acoustics, Rome, Italy, 2-7 September 2001, Ed. A. Alippi (2001), Vol. 1, pp. 270-271.

8. D. J. O'Boy, E.P. Bowyer, V.V. Krylov, *Damping of flexural vibrations in thin plates using one and two dimensional acoustic black hole effect*, in: Proceedings of the 10th International Conference on Recent Advances in Structural Dynamics (RASD 2010), Southampton, UK, 12-14 July 2010, [CDROM].
9. V. V. Krylov, R.E.T.B. Winward, *Experimental investigation of the acoustic black hole effect for flexural waves in tapered plates*, in: Journal of Sound and Vibration, Vol. 300 (2007), pp. 43-49.
10. E. P. Bowyer, J.M. Lister, V.V. Krylov, D.J. O'Boy, *Experimental study of damping flexural vibrations in tapered turbofan blades*, in: Proceedings of the conference 'Acoustics 2012', Nantes, France, 23-27 April 2012, pp. 2201- 2206.
11. V. V. Krylov, *Propagation of plate bending waves in the vicinity of one- and two-dimensional acoustic 'black holes'*, in: Proceedings of the ECCOMAS International Conference on Computational Methods in Structural Dynamics and Earthquake Engineering (COMPDYN 2007), Rethymno, Crete, Greece, 13-16 June 2007, [CD-ROM].
12. P. A. Feurtado, S. C. Conlon, *Experimental analysis of vibration and radiated sound power reduction using an array of acoustic black holes*, in: *Proceedings of the 44th Inter-Noise Congress & Exposition on Noise Control Engineering "Internoise2015"*, San Francisco, California, USA, 9-12 August 2015, [CD-ROM].
13. F. Gautier, J. Cuenca, V.V. Krylov, L. Simon, *Experimental investigation of the acoustic black hole effect for vibration damping in elliptical plates (Abstract for the Conference "Acoustics 08", Paris, France, June 2008)*, Journal of the Acoustical Society of America, Vol. 123, No 5 (2008) p. 3318.

14. E. P. Bowyer, D.J. O'Boy, V.V. Krylov, F. Gautier, *Experimental investigation of damping flexural vibrations using two-dimensional acoustic 'black holes'*, in: Proceedings of the International conference on Noise and Vibration Engineering (ISMA 2010), Leuven, Belgium, 20-22 September 2010 (Ed. P. Sas, B. Bergen) (2010), pp. 1181-1192.
15. S. C. Conlon, J. B. Fahline, F. Semperloti, P. A. Feurtado, *Enhancing the low frequency vibration reduction performance of plates with embedded Acoustic Black Holes*, in: *Proceedings of the 43rd Inter-Noise Congress & Exposition on Noise Control Engineering "Internoise2014"*, Melbourne, Australia, 16-19 November 2014, [CD-ROM].
16. E. P. Bowyer, D. J. O'Boy, V. V. Krylov, *Damping of flexural vibrations in composite plates and panels containing one- and two-dimensional acoustic black holes*, in: Proceedings of the conference 'Acoustics 2012', Nantes, France, 23-27 April 2012, pp. 2193-2198.
17. L. Zhao, S. C. Conlon, R. Semperlotti, *Experimental verification of the energy harvesting performance performance in plate-like structures with embedded acoustic black holes,* in: *Proceedings of the 44th Inter-Noise Congress & Exposition on Noise Control Engineering "Internoise2015"*, San Francisco, California, USA, 9-12 August 2015, [CD-ROM].
18. M. A. Mironov, V. V. Pislyakov, *One-dimensional acoustic waves in retarding structures with propagation velocity tending to zero*, Acoustical Physics, Vol. 48 (3) (2002), pp. 347–352.
19. O. Umnova, B. Zajamsek, *Omnidirectional graded index sound absorber*, in: Proceedings of the conference 'Acoustics 2012', Nantes, France, 23-27 April 2012, pp. 3631-3637.

20. L. Cremer, M. Heckl and E.E. Ungar, *Structure-Borne Sound, Structural Vibrations and Sound Radiation at Audio Frequencies*. (Springer-Verlag, Berlin Heidelberg New York, 1973).
21. J.S. Bendat, A.G. Piersol, *Random Data Analysis and Measurement Procedures*, Third Edition, (Wiley Inter-Science, John Wiley & Sons, New York, 2000).
22. K.T. Brown and M.P. Norton, *Some comments on the experimental determination of modal densities and loss factors for statistical energy analysis applications*, J. Sound Vib. 102(4), 588-594 (1985).
23. P.R. Keswick and M.P. Norton, *A comparison of modal density measurement techniques*, Applied Acoustics 20, 137-153 (1987)
24. J. Segelstein, "And you think you're trying to save gas …," *NBC News*. NBC, 10 July 2008.

ACADEMIC VITA of Angelina M. Conti
angelinaconti2@gmail.com

Education:

The Pennsylvania State University, University Park, PA
Bachelor of Science in Aerospace Engineering, Spring 2016
Schreyer Honors College

Honors Thesis: Vibration Damping of Aluminum Plates using Acoustic Black Holes for Application in Aerospace Structures
Thesis Advisor: Dr. Stephen C. Conlon
Honors Advisor: Dr. Dennis K. McLaughlin

International Education:

Tecnun – Universidad de Navarra
Study Abroad, May 2013

Work Experience:

Structural Vibrations, The Pennsylvania State University (Spring 2013 – present)
Advisor: Dr. Stephen C. Conlon (University Park, PA)

Flight Vehicle Design and Fabrication, Human Powered Aircraft, The Pennsylvania State University (Spring 2013 – present)
Advisor: Dr. Mark D. Maughmer (University Park, PA)

Aerodynamics Undergraduate Teaching Internship, The Pennsylvania State University (Fall 2015)
Advisor: Dr. Sven Schmitz (University Park, PA)

Advanced Conceptual Design Internship, The Boeing Company (Summer 2015)
Supervisor: Eric Brown (Long Beach, CA)

IT FLIES USA Competition, Merlin Flight Simulation Group (Spring 2014 – Spring 2015)
Supervisor: Dr. Mark D. Maughmer

Conceptual Design Internship, The Boeing Company (Summer 2014)
Supervisor: Ken Perez (Everett, WA)

Technical Support Internship, General Electric: Transportation (Summer 2013)
Supervisor: Brian Darold (Erie, PA)

Honors and Awards:

William & Wyllis Leonhard Engineering Scholars Program
Penn State Engineering Design Showcase Best Design Communication Award
The Boeing Company Scholarship
Pyle Leslie & Anna Memorial Scholarship
Schumacher Honors Scholarship
Sigma Gamma Tau
Dean's List, all semesters

Professional Memberships:

Student Member, American Institute of Aeronautics and Astronautics